Phase-contrast X-ray microtomography of mouse fetus

Masato Hoshino, Kentaro Uesugi and Naoto Yagi*

Japan Synchrotron Radiation Research Institute, SPring-8, 1-1-1 Kouto, Sayo, Hyogo 679-5198, Japan

*Author for correspondence (yagi@spring8.or.jp)

Biology Open 1, 269–274
doi: 10.1242/bio.2012430

Summary

A phase-contrast X-ray microtomography system using the Talbot imaging has been built at the SPring-8 synchrotron radiation facility. This system has much higher density resolution than absorption-based X-ray microtomography. The tomographic sections of formalin-fixed mouse fetuses obtained with this method clearly depict various organs without any staining at a pixel resolution of up to 5 μm. Since this technique allows us to obtain three-dimensional structural information without sectioning, it will be particularly useful to examine anomalies that take place during development. It can be also used to quantitatively measure volume and mass of organs during development.

Key words: Phase-contrast, X-ray CT, Fetus

Introduction

Mouse is one of the most important, frequently used experimental animals. Especially, transgenic mice are now regarded as a common tool to investigate functions of proteins *in vivo*. Mouse fetuses are extensively studied to determine the roles of genes in development and congenital abnormalities. With an increase of new transgenic animals, effective methods to identify novel phenotypes in these fetuses are crucial. However, detailed examination of a mouse fetus in the past has involved thin sectioning for observation under a microscope.

Several 3D imaging techniques at micron-resolution have been reported for observation of an embryo or a fetus. (1) Magnetic resonance microscopy has been used extensively (Cleary et al., 2011; Petiet et al., 2008; Smith et al., 1994). The resolution now reaches about 10 μm. The contrast in magnetic resonance microscopy is not directly related to a physical parameter of the material but distinguished contrast is observed among organs. (2) Johnson et al. (Johnson et al., 2006) reported X-ray microscopic computed tomography (microCT) at 8 μm resolution. Since a mouse fetus is mostly made of soft tissues, only poor contrast is obtained by absorption-based X-ray CT of a native fetus. Thus, they employed extensive staining by osmium. The organs and tissues may be differentiated by different methods of staining. (3) Sharpe (Sharpe, 2003) introduced optical projection tomography (OPT) as a new tool for studying fetus anatomy. A fetus is made transparent chemically and then stained with various dyes. Since the sample can be selectively stained, it is possible to study specific structures such as vascular development (Walls et al., 2008) or gene expression patterns (Summerhurst et al., 2008). (4) Although destructive, episcopic techniques are also widely used (Weninger and Geyer, 2008). (5) Ultrasound is the most common method to examine a human fetus *in vivo*. High-frequency ultrasound biomicroscopy (UBM) has a spatial resolution of 30–50 μm and is particularly useful in visualizing blood flow in a fetus (Phoon, 2006). (6) Although the penetration depth is limited, optical coherence tomography (OCT) has a resolution better than 10 μm (Luo et al., 2006; Syed et al., 2011). It is also powerful in studying cardiovascular development (Larina et al., 2008).

Here we present yet another technique to visualize development. Phase-contrast X-ray CT is an emerging imaging technique that makes use of X-ray phase-shift in biological tissues (Momose, 2005). Since the X-ray phase-shift cross sections are about 1000 times larger than the X-ray absorption cross-sections for low Z elements such as hydrogen, carbon, nitrogen, and oxygen, phase-contrast X-ray CT enables us to visualize the density distribution in biological soft tissues with a much higher contrast than conventional X-ray CT (Momose, 2005; Momose et al., 1996). This technique has been used in structural studies of soft tissues such as brain (McDonald et al., 2009; Noda-Saita et al., 2006; Pfeiffer et al., 2007; Schulz et al., 2010), liver (Wu et al., 2009), atherosclerotic plaque (Shinohara et al., 2008) and eye lens (Hoshino et al., 2010; Hoshino et al., 2011). Since an embryo and a fetus before bone calcification are made mostly of soft tissues, this technique is suitable for these samples. In this paper, results from first studies on mouse fetuses are presented.

Materials and Methods

Phase-contrast X-ray imaging makes use of phase shift of X-rays. When an X-ray passes through an object, the phase of the X-ray changes. The amount of phase shift is the sum of phase shifts caused by the materials through which the X-ray propagates. The phase shift caused by each material is linearly related to its refractive index to X-rays, which in turn is roughly proportional to its density when the material contains only low Z elements. This situation is analogous to the radiogram but phase shift is utilized in place of absorption. Thus, as in X-ray CT, tomographic reconstruction is feasible from images obtained at different angles of the sample. Since phase shift is more sensitive to difference in density than absorption, higher density contrast is obtained.

To measure phase difference for imaging, we use a grating-based interferometer ("Talbot" type, (Momose et al., 2003)) (Fig. 1). This interferometer is placed at the BL20B2 beamline (Goto et al., 2001) in the SPring-8 synchrotron radiation facility (Hyogo, Japan), which uses a bending magnet of the storage ring as an X-ray source. The X-rays with a wide spectrum are monochromatized by a silicon double-crystal monochromator in the optics hutch. The beamline covers an energy range of 8 to 100 keV. There are two experimental stations, one in the storage ring

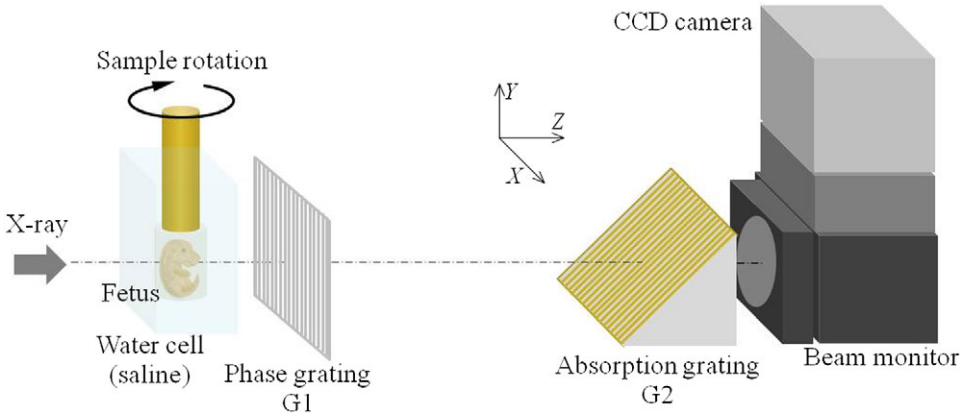

Fig. 1. The experimental setup for Talbot phase-contrast imaging at BL20B2 in SPring-8. The sample is soaked in a cell filled with phosphate-buffered saline which has windows to pass the X-ray.

building at 45 m from the source and the other in a separate building of the biomedical imaging center at 203 m. At the 45 m hutch, the X-ray intensity is about 4×10^9 photons/s/mm^2 and the beam size is about 60 mm (width) by 4 mm (height) at 30 keV. At the 203 m hutch, the beam is much larger (300 mm (width) by 20 mm (height)) but the intensity is about 20 times lower. Thus, for small samples, the measurement should be done in the 45 m hutch to obtain high spatial resolution. For large samples, the larger beam in the 203 m hutch is required.

The Talbot grating interferometer has two transmission gratings: a phase grating (G1) and an absorption grating (G2) (Fig. 1). Grating parameters and materials were varied depending on the size of the fetus sample. There is a trade-off between spatial resolution and the field of view. For embryos of 6 and 9 days which were imaged in the 45 m hutch, both gratings were made of tantalum and the pattern thickness of G1 and G2 was 0.96 µm and 4.75 µm, respectively. The pitch of both gratings was 5 µm and the grating area size was 5 mm (width) by 10 mm (height). G2 was inclined by 60° towards the beam so as to increase the effective X-ray absorption by the grating. The X-ray imaging detector consisted of a "beam-monitor" and a charge coupled device (CCD) camera. For fetuses of 6 and 9 days, the "beam monitor" was composed of a 10 µm-thick P43 (Gd_2O_2S:Tb) phosphor screen and a f=50 mm lens. The camera was a fast read-out CCD camera (C9100-02, Hamamatsu Photonics, Hamamatsu, Japan) equipped with a f=85 mm lens. The effective pixel size was 4.9 µm. For fetuses of 10, 11, 13, 15 days which were imaged at the 203 m hutch, grating G1 was made of tantalum and G2 was made of gold with pattern thicknesses 2.1 µm and 16.6 µm, respectively. The pitch of both gratings was 10 µm and the grating area size was 25 mm (width) by 25 mm (height). The inclination angle of G2 was 45°. The "beam monitor" was composed of a 20 µm-thick P43 phosphor screen and a f=105 mm lens. The CCD camera (C4880-41S, Hamamatsu Photonics, Hamamatsu. Japan) was equipped with a f=105 mm lens. In this case, the effective pixel size was 5.87 µm per pixel. In the actual measurement, a CCD camera was used in the binning mode (4×4 binning with 23.5 µm pixels).

Measurement with the interferometers with phase stepping (done by shifting the G2 grating horizontally across the beam) provides a projection image of phase-shifts. Since the phase-shifts by the materials are added along the X-ray path, it is possible to apply the tomographic technique (Radon transformation). After tomographic reconstruction, the value of X-ray refractive index in each cubic voxel was determined by the calibration procedure with salt solutions of known density as described (Hoshino et al., 2010; Hoshino et al., 2011). In the present study, the calibration was made with five solutions: water (1.000 g/cm^3), normal saline (1.006 g/cm^3), and salt solutions of 1.051, 1.110, 1.143 g/cm^3. The correlation between the measured and calculated densities was R^2=0.9961. The density resolution, which was estimated from the pixel values in the saline, was 3.9 mg/cm^3 (3σ) in the present experiment. Since the X-ray refractive index is related to the number of electrons in a volume, it is necessary to know the mean ratio of atomic number-to-mass of the material to convert it to density. This ratio is given as 0.547 for eye lens in the National Institute for Standard database (http://physics.nist.gov/PhysRefData/XrayMassCoef/tab2.html). The value for liver is not given, but as it is 0.552 for brain and 0.550 for skeletal muscle, we assumed 0.550.

Reconstruction of the CT slices was done with a home-made original software. Further image processing of the CT data was performed with ImageJ (http://rsbweb.nih.gov/ij/index.html) and a home-made software "slice" (http://www-bl20.spring8.or.jp/slice/index.html). Segmentation of liver was done manually with Photoshop (Adobe, San Jose, CA, USA).

The samples were taken from pregnant BALB/C mice (CLEA Japan, Inc., Tokyo). In the case of embryos of 6, 9 and 10 days, uterus was cut to separate fetuses and they were imaged in the intact uterus wall and amnion. The fetuses were fixed in phosphate buffered formalin (pH 7.0) without any staining and then soaked in low-temperature melting agar at around 38℃ and embedded. The block of agar was attached to the rotating axis for tomography. Larger fetuses were either taken from uterus or left in uterus and fixed and embedded in agar. The images were acquired at 0.2degree intervals (900 projections) or 0.3degree intervals (600 projections) with five phase steps. The animal experiments were conducted with a permission from the SPring-8 Animal Care and Welfare Committee.

Results

Fig. 2 shows a cross section of mouse uterus at a gestational day of 6. Only the egg cylinder and remains of uterine lumen (with higher density) can be observed. Fig. 3 shows approximately sagittal tomographic sections of mouse fetuses at gestational days of 9, 10, 11, 13 and 15. At day 9, the fetus is strongly flexed in a dorsally convex direction. At the center of the embryo is the heart in the early development stage. Other organs are not identifiable but it is clear that the present technique allows us to visualize details of the early development. In Fig. 2, 32 somites can be counted at 11 days, and most of the major organs, such as brain tube, heart, liver, stomach, intestine, are visible, among which liver has the highest density. At 13 days, compared with adult mouse the head is disproportionately large. However, brain is still

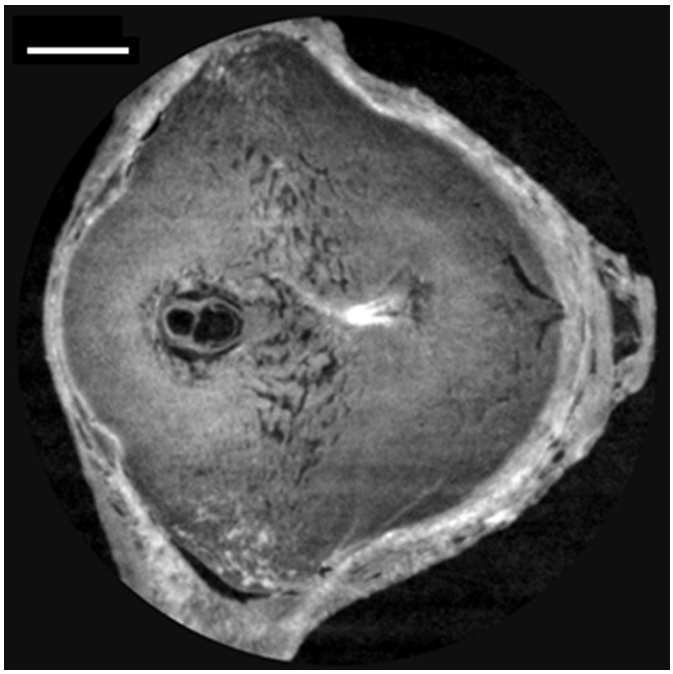

Fig. 2. A cross section of a mouse uterus at a gestational day of 6. The scale bar is 1 mm.

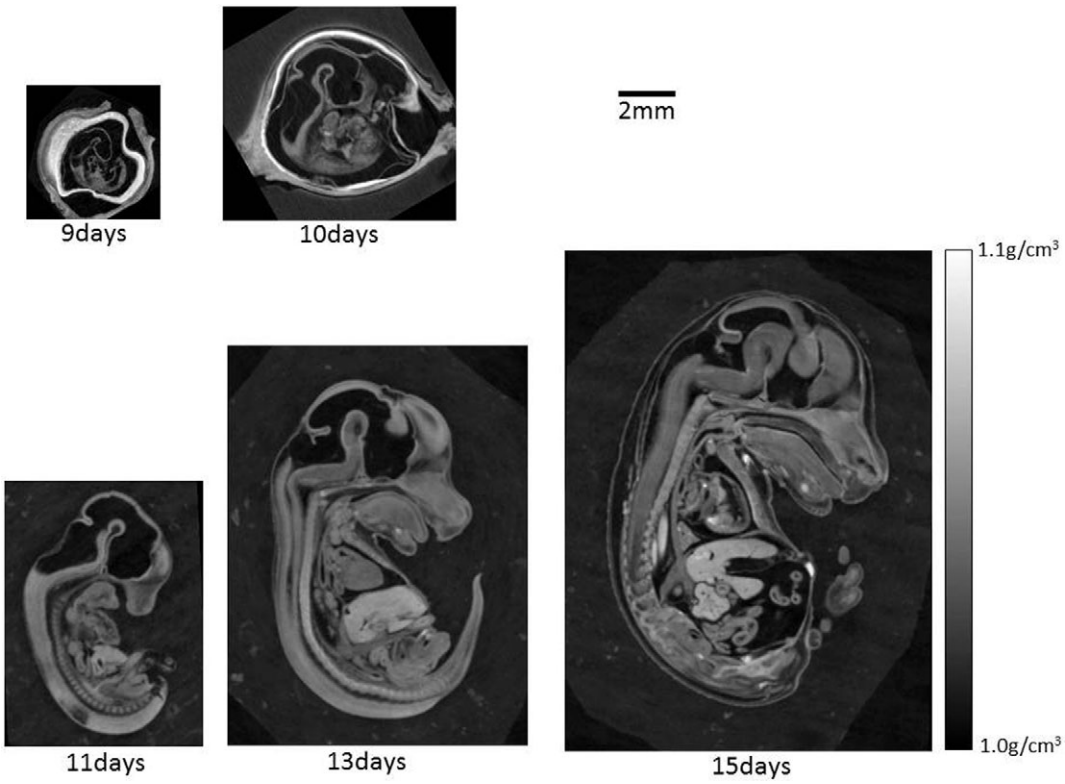

Fig. 3. Tomographic sections of mouse fetuses at gestational days of 9, 10, 11, 13 and 15.

undeveloped and large ventricles occupy the major part of the head. On the other hand, tongue and palatal process are well developed and Meckel's cartilage is present. Chondrification of vertebrate column is still in process at 15 days. All these features are well correlated with microscopic observations of stained sections (Theiler, 1989).

Fig. 4a shows a cross section of a 13 day fetus recorded with an absorption-based high resolution CT. The sample-to-detector distance was 3 m so that the edge-enhancement due to refraction of X-rays was effective (Yagi et al., 1999). Although this technique is powerful in visualization of lung and bone which have high density variations, the contrast in fetus is very low. Compared with this, it is clear that the phase-contrast CT has a great advantage in density resolution. Fig. 4b shows umbilical hernia in the 13 day fetus, which is normal during this period (Kaufman, 1992). Fig. 5 shows a series of lateral sections from thorax to abdomen of the 15 day fetus. Sections of lungs, heart, liver, intestine and kidneys are clearly visualized. The details of the forelegs are also depicted. The high density spots in liver and lungs are probably coagulated blood.

Eye is one of the organs that are best visualized by phase-contrast X-ray imaging (Hoshino et al., 2010; Hoshino et al., 2011). The density of lens increases with gestational days (Table 1) and the cross-sections of lenses at 11, 13 and 15 days (Fig. 6) show that the density distribution is non-uniform, with higher density at the distal side and sometimes lower at the axis than in the lateral sides (Fig. 5c). The highest density in the lens of the 15 day fetus was about 1.12 g/cm^3. This is still much lower than the density at the center of an adult lens (1.27 g/cm^3 (Hoshino et al., 2010; Hoshino et al., 2011)). Thus, the protein (crystallin) is still being concentrated. Although mouse eyes can be studied in uterus *in vivo* by ultrasound biomicroscopy (Foster et al., 2003), precise density measurement with an accuracy better than 0.3% (Table 1) is only possible with the present

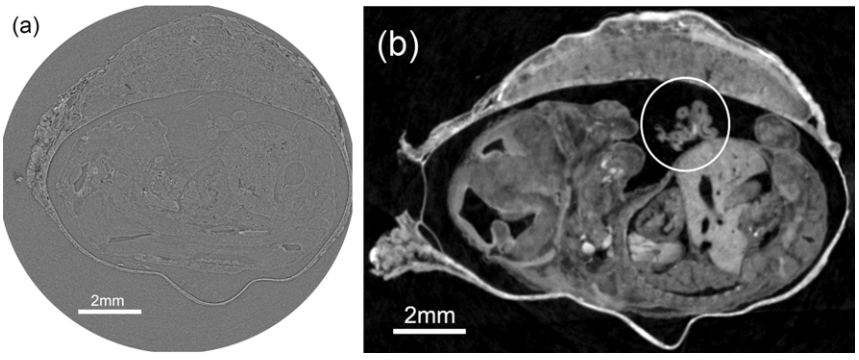

Fig. 4. Images of a 13 day fetus. (a) Image taken with absorption-based micro CT. The sample-to-detector distance was 3 m so that edge-enhancement by refraction of X-rays was utilized. Apart from the omission of the gratings, the experimental conditions were identical with the phase-contrast CT. (b) Umbilical hernia in the 13 day fetus (circle) recorded with phase-contrast CT.

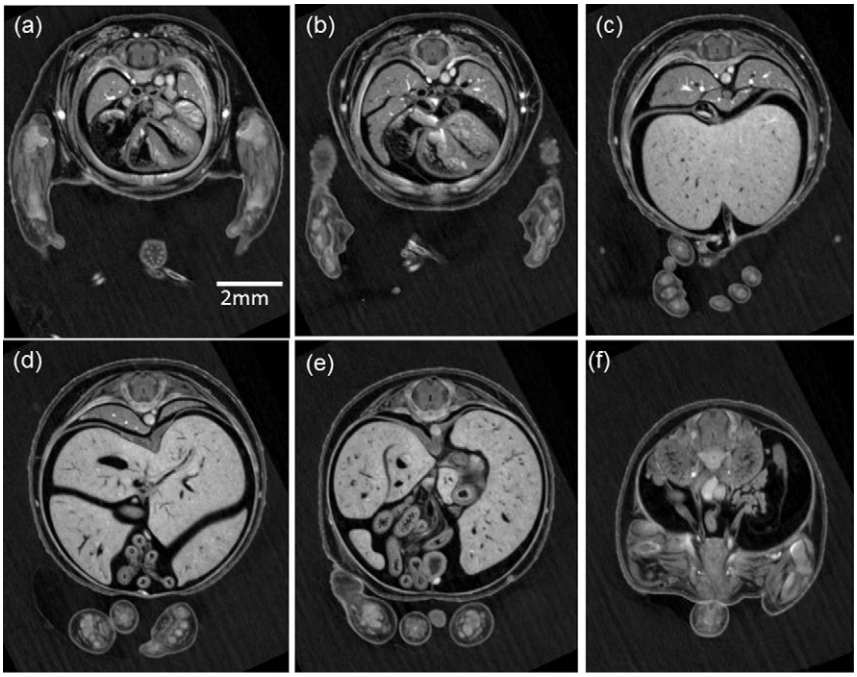

Fig. 5. Tomographic lateral sections from thorax to abdomen of a 15 day mouse fetus.

Table 1. Density of eye lens at different gestational days.

gestational days	10 days	11 days	13 days	15 days
density (g/cm^3)	1.043±0.003	1.055±0.002	1.058±0.002	1.071±0.002

Two lenses of a mouse for each gestational day were measured. These values were obtained by averaging density across a lens along a line that passed through its center. Means and the standard deviations were obtained over ten consecutive slices of a specimen, except five slices in the 10 day fetus in which the lens was not large enough for ten slices.

technique. It enables us not only to measure the density more accurately than before but to examine the protein density profile that is important for the function (focusing) of the lens (Hoshino et al., 2011). This finding on the density and its distribution in mouse lens during development is completely new and more detailed work is in progress.

One unique feature of phase-contrast X-ray CT is its high quantitativeness (Hoshino et al., 2010), which enables us to measure density of organs quantitatively. As an example, the volume and the mass of liver were measured (Table 2). The volume of liver increased by more than 10 times in four days from gestational days of 11 to 15, while its density remained more or less constant. In adult mice, the liver weight is about 5% of the body weight (according to the data taken from the supplier of the mice), while it is more than 10% even on day 15 when the body weight was about 400 mg, demonstrating that development of liver precedes that of the whole body (Theiler, 1989). Although the measurement was made only in one specimen for each gestation day, the accuracy of the each obtained value is better than 1% (see Materials and Methods). Much larger errors are expected from the segmentation procedure and there is also individual variability among fetuses of the same gestation day (even among littermates) (Bijlani et al., 1980).

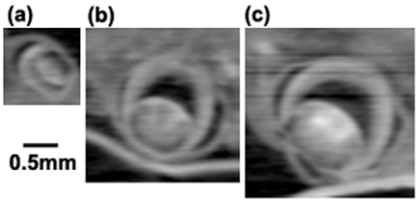

Fig. 6. Cross-sections of eyes at (a) 11, (b) 13 and (c) 15 gestational days of a mouse fetus.

Discussion

With an absorption-based X-ray CT system including those in hospitals, it is necessary to use a contrast agent to visualize organs except bone and lung *in vivo*. Similarly, staining with heavy elements is required for *ex vivo* experiments. The phase-contrast X-ray CT, which has a contrast resolution of 3.6 mg/ml (Momose et al., 2005), makes it possible to visualize most of the organs clearly without a contrast agent or staining.

Table 2. Volume, mass and density of liver in mouse fetuses.

gestational days	11 days	13 days	15 days
volume (mm^3)	4.1	27.3	55.2
mass (mg)	4.3	28.8	57.5
density (g/cm^3)	1.054	1.054	1.041

One fetus for each gestational day was analyzed. Segmentation was done manually in each slice with Photoshop (Adobe, San Jose, CA, USA).

Transgenic animals are widely used in medical investigations. Not only to create a "knock-out" mouse that lacks a particular protein, it is now possible to control the expression of a particular protein in a specific cell. However, when a gene is modified, the animal often dies preterm before birth. In such a case, it is important to ascertain the cause of the premature death. A fetus before bone calcification is wholly a soft tissue without air and thus suitable for phase contrast X-ray tomography. It is easy to find anatomical differences in the transgenic animal and deduce the problem. Since a mouse fetus is very small, an anatomical study requires troublesome embedding, staining and sectioning that require high skills. Even with these efforts, it is hard to get three-dimensional anatomical information. With computed tomography, sections in any direction can be easily obtained at a resolution similar to that of microscopy (Fig. 2). Moreover, since a fetus can be imaged within uterus, manipulation of the sample is unnecessary and simple formalin fixation is sufficient, reducing the possibility of sample damages during preparation. Thus, it saves a plenty of time and efforts for sample preparation, making it possible to work on fetuses of various transgenic animals in an automated system.

The most notable advantage of phase-contrast X-ray CT is its high quantitativeness. The density measurements of liver and lens (Tables 1 and 2) make use of this advantage. The high density resolution facilitates identification of organs and tissues, but automated segmentation software is necessary to make the best of this advantage.

Phase-contrast X-ray CT does not require any staining. In this respect, it is similar to magnetic resonance microscopy. The extensive staining that was employed by Johnson et al. (Johnson et al., 2006) for absorption-based microCT is unnecessary for phase-contrast microCT. On the other hand, it is difficult to stain the sample to visualize specific materials of interest such as proteins and RNAs. It is possible to use a low concentration of a contrast agent to visualize the cardiovascular system. Another limitation of phase-contrast X-ray CT is that materials with too high density (such as calcified bone) or too low density (such as air) causes artifacts in the reconstructed image as is the case in OPT, which makes it difficult to visualize an *in vivo* fetus. This is due to the high density resolution and the limited dynamic range, and can be avoided by using high energy X-rays with some deterioration in the density resolution.

Johnson et al. (Johnson et al., 2006) compared several methods for embryo phenotype screening. Although the cost/sample is hard to compare because of the changes in the instrument prices, synchrotron radiation in the hard X-ray range, which is obtainable only in a small number (currently about 30) of facilities in the world, is clearly a limited resource. At the moment, the phase-contrast CT is routinely available only in ESRF (Grenoble, France), SLS (Villigen, Switzerland) and SPring-8 (Hyogo, Japan). However, since its potential is being recognized, more facilities are implementing the technique now. Most facilities provide beam time free for academic researches, and for such simple imaging as described in this paper, data collection by "mail-in" may be possible. For the present study, it took 1–2 hours to scan each sample at a spatial resolution of 10–20 μm. However, this can be much reduced, to as short as one second, by using a multilayer monochromator or a white beam to increase flux (McDonald et al., 2009; Momose et al., 2009b). For a screening purpose, high-speed scan will be essential. Since the Talbot imaging does not require a monochromatic X-ray, there is a possibility that a laboratory apparatus may be realized in future (Momose et al., 2009a; Pfeiffer et al., 2006).

At SPring-8, absorption-based microCT is used to study meteorites (Nakamura et al., 2008). In those studies, microCT is used to obtain a gross 3D structure nondestructively. Then, after locating the region of interest (ROI), the sample is cut at an appropriate position to reveal an interesting cross-section, and investigations are made to identify the materials in the ROI. This is the best way to make use of the nondestructive nature of tomographic techniques. For example, to find out the cause of preterm death of a transgenic mouse, it is feasible to identify anomalies with phase-contrast CT and then section the fetus in an appropriate direction. The section can be stained using a variety of techniques for further histological analysis.

Acknowledgements

We thank Prof. S. Mohri of Okayama University Faculty of Medicine during the early stage of this study, Prof. B. Pierscionek of University of Ulster UK for discussion on the lens development, and our colleague Dr. H. Iwamoto for help with the fetus samples. The experiment at SPring-8 was performed with an approval of the Japan Synchrotron Radiation Research Institute (2010A1450, 2010B1293). This work was supported by Intramural Research Fund 11-1-2 for Cardiovascular Diseases of National Cerebral and Cardiovascular Center.

Competing Interests

The authors declare no competing interests.

References

Bijlani, V., Grewal, M. S. and Rao, K. (1980). Birth weight and development of cerebellar cortex. *J. Anat.* **130**, 769-775.

Cleary, J. O., Modat, M., Norris, F. C., Price, A. N., Jayakody, S. A., Martinez-Barbera, J. P., Greene, N. D., Hawkes, D. J., Ordidge, R. J., Scambler, P. J. et al. (2011). Magnetic resonance virtual histology for embryos: 3D atlases for automated high-throughput phenotyping. *NeuroImage* **54**, 769-778.

Foster, F. S., Zhang, M., Duckett, A. S., Cucevic, V. and Pavlin, C. J. (2003). In Vivo Imaging of Embryonic Development in the Mouse Eye by Ultrasound Biomicroscopy. *Invest. Ophthalmol. Vis. Sci.* **44**, 2361-2366.

Goto, S., Takeshita, K., Suzuki, Y., Ohashi, H., Asano, Y., Kimura, H., Matsushita, T., Yagi, N., Isshiki, M., Yamazaki, H. et al. (2001). Construction and commissioning of a 215-m-long beamline at SPring-8. *Nucl. Instrum. Methods Phys. Res. Sect. A* **467-468**, 682-685.

Hoshino, M., Uesugi, K., Yagi, N. and Mohri, S. (2010). *Investigation of Imaging Properties of Mouse Eyes Using X-ray Phase Contrast Tomography*, Vol. 1266, pp. 57-61. New York: American Institute of Physics.

Hoshino, M., Uesugi, K., Yagi, N., Mohri, S., Regini, J. and Pierscionek, B. (2011). Optical properties of *in situ* eye lenses measured with X-ray Talbot interferometry. *PLoS ONE* **6**, e25140.

Johnson, J. T., Hansen, M. S., Wu, I., Healy, L. J., Johnson, C. R., Jones, G. M., Capecchi, M. R. and Keller, C. (2006). Virtual Histology of Transgenic Mouse Embryos for High-Throughput Phenotyping. *PLoS Genet.* **2**, e61.

Kaufman, M. H. (1992). *The Atlas of Mouse Development*. New York: Academic Press.

Larina, I. V., Sudheendran, N., Ghosn, M., Jiang, J., Cable, A., Larin, K. V. and Dickinson, M. E. (2008). Live imaging of blood flow in mammalian embryos using Doppler swept-source optical coherence tomography. *J. Biomed. Opt.* **13**, 060506.

Luo, W., Marks, D. L., Ralston, T. S. and Boppart, S. A. (2006). Three-dimensional optical coherence tomography of the embryonic murine cardiovascular system. *J. Biomed. Opt.* **11**, 021014.

Mcdonald, S. A., Marone, F., Hintermüller, C., Mikuljan, G., David, C., Pfeiffer, F. and Stampanoni, M. (2009). Advanced phase-contrast imaging using a grating interferometer. *J. Synchrotron Radiat.* **16**, 562-572.

Momose, A. (2005). Recent Advances in X-ray Phase Imaging. *Jpn. J. Appl. Phys.* **44**, 6355-6367.

Momose, A., Takeda, T., Itai, Y. and Hirano, K. (1996). Phase-contrast X-ray computed tomography for observing biological soft tissues. *Nat. Med.* **2**, 473-475.

Momose, A., Kawamoto, S., Koyama, I., Hamaishi, Y., Takai, K. and Suzuki, Y. (2003). Demonstration of X-Ray Talbot Interferometry. *Jpn. J. Appl. Phys* **42**, L866-L868.

Momose, A., Fujii, A., Kadowaki, H. and Jinnai, H. (2005). Three-dimensional observation of polymer blend by X-ray phase tomography. *Macromolecules* **38**, 7197-7200.

Momose, A., Yashiro, W., Kuwabara, H. and Kawabata, K. (2009a). Grating-Based X-ray Phase Imaging Using Multiline X-ray Source. *Jpn. J. Appl. Phys* **48**, 076512.

Momose, A., Yashiro, W., Maikusa, H. and Takeda, Y. (2009b). High-speed X-ray phase imaging and X-ray phase tomography with Talbot interferometer and white synchrotron radiation. *Opt. Express* **17**, 12540-12545.

Nakamura, T., Noguchi, T., Tsuchiyama, A., Ushikubo, T., Kita, N. T., Valley, J. W., Zolensky, M. E., Kakazu, Y., Sakamoto, K., Mashio, E. et al. (2008). Chondrulelike Objects in Short-Period Comet 81P/Wild 2. *Science* **321**, 1664-1667.

Noda-Saita, K., Yoneyama, A., Shitaka, Y., Hirai, Y., Terai, K., Wu, J., Takeda, T., Hyodo, K., Osakabe, N., Yamaguchi, T. et al. (2006). Quantitative Analysis of Amyloid Plaques in a Mouse Model of Alzheimer's Disease by Phase-Contrast X-ray Computed Tomography. *Neuroscience* **138**, 1205-1213.

Petiet, A. E., Kaufman, M. H., Goddeeris, M. M., Brandenburg, J., Elmore, S. A. and Johnson, G. A. (2008). High-resolution magnetic resonance histology of the embryonic and neonatal mouse: A 4D atlas and morphologic database. *Proc. Natl. Acad. Sci. USA* **105**, 12331-12336.

Pfeiffer, F., Weitkamp, T., Bunk, O. and David, C. (2006). Phase retrieval and differential phase-contrast imaging with low-brilliance X-ray sources. *Nat. Phys.* **2**, 258-261.

Pfeiffer, F., Bunk, O., David, C., Bech, M., Le Duc, G., Bravin, A. and Cloetens, P. (2007). High-resolution brain tumor visualization using three-dimensional x-ray phase contrast tomography. *Phys. Med. Biol.* **52**, 6923-6930.

Phoon, C. K. (2006). Imaging tools for the developmental biologist: ultrasound biomicroscopy of mouse embryonic development. *Pediatr. Res.* **60**, 14-21.

Schulz, G., Weitkamp, T., Zanette, I., Pfeiffer, F., Beckmann, F., David, C., Rutishauser, S., Reznikova, E. and Müller, B. (2010). High-resolution tomographic imaging of a human cerebellum: comparison of absorption and grating-based phase contrast. *J. R. Soc. Interface* **7**, 1665-1676.

Sharpe, J. (2003). Optical projection tomography as a new tool for studying embryo anatomy. *J. Anat.* **202**, 175-181.

Shinohara, M., Yamashita, T., Tawa, H., Takeda, M., Sasaki, N., Takaya, T., Toh, R., Takeuchi, A., Ohigashi, T., Shinohara, K. et al. (2008). Atherosclerotic plaque imaging using phase-contrast X-ray computed tomography. *Am. J. Physiol.* **294**, H1094-H1100.

Smith, B. R., Johnson, G. A., Groman, E. V. and Linney, E. (1994). Magnetic resonance microscopy of mouse embryos. *Proc. Natl. Acad. Sci. USA* **91**, 3530-3533.

Summerhurst, K., Stark, M., Sharpe, J., Davidson, D. and Murphy, P. (2008). 3D representation of Wnt and Frizzled gene expression patterns in the mouse embryo at embryonic day 11.5 (Ts19). *Brain Res. Gene Expr. Patterns* **8**, 331-348.

Syed, S. H., Larin, K. V., Dickinson, M. E. and Larina, I. V. (2011). Optical coherence tomography for high-resolution imaging of mouse development in utero. *J. Biomed. Opt.* **16**, 046004.

Theiler, K. (1989). *The House Mouse: Atlas of Embryonic Development*. New York: Springer-Verlag.

Walls, J. R., Coultas, L., Rossant, J. and Henkelman, R. M. (2008). Three-Dimensional Analysis of Vascular Development in the Mouse Embryo. *PLoS ONE* **3**, e2853.

Weninger, W. J. and Geyer, S. H. (2008). Episcopic 3D Imaging Methods: Tools for Researching Gene Function. *Curr. Genomics* **9**, 282-289.

Wu, J., Takeda, T., Lwin, T. T., Momose, A., Sunaguchi, N., Fukami, T., Yuasa, T. and Akatsuka, T. (2009). Imaging renal structures by X-ray phase-contrast microtomographyX-ray phase-contrast microtomogram of APA hamster. *Kidney Int.* **75**, 845-951.

Yagi, N., Suzuki, Y., Umetani, K., Kohmura, Y. and Yamasaki, K. (1999). Refraction-enhanced x-ray imaging of mouse lung using synchrotron radiation source. *Med. Phys.* **26**, 2190-2193.